AIAA JOURNAL
Vol. 42, No. 11, November 2004

Nonlinear Modeling of Delaminated Struts

G. W. Hunt,* B. Hu,† R. Butler,‡ D. P. Almond,§ and J. E. Wright¶
University of Bath, Bath, England BA2 7AY, United Kingdom

A phenomenological overview of the buckling and postbuckling of fully and partially delaminated struts is developed using a simple four-degree-of-freedom nonlinear Rayleigh–Ritz formulation. Bifurcation analysis indicates that instability occurs in general at an asymmetric point of bifurcation. After bifurcation, realistic solutions are seen to follow the stable part of the postbuckling path, with the unstable branch being denied by contact between the contributing laminates. Depending on the geometry and position of the delamination, thoroughly stable (thin-film), effectively neutral (overall), or potentially unstable (mixed-mode) buckling can occur in the postbuckling range. Numerically obtained equilibrium solutions of the model are found to compare well with those obtained using the finite element code ABAQUS. Critical delamination depths, where the response undergoes a change in form, are discovered at positions of secondary bifurcation. The multiplicity of equilibrium solutions that arise at such points are seen to cause possible problems of path selection for standard finite element routines.

I. Introduction

THE possibility of invisible or barely visible delamination damage after low velocity impact from relatively small objects is causing concern in aerospace design, where it is known to result in significant reductions in strength. Most design problems relate to plates rather than struts, and yet it is worth noting that for undelaminated systems, with the important addition of nonlinear in-plane stretching effects, extended strut models have provided a good introduction to plate buckling.[1,2] However, the delaminated strut, unlike its prismatic counterpart, exhibits nonlinear stretching effects that are comparable to those found in plate and shell structures. These lead to a postbuckling response initiated at an asymmetric or transcritical point of bifurcation, where the stable postbuckling direction is marked by separation of the two laminates, whereas the unstable route is denied by their inability to pass through one another.

A four-degree-of-freedom, Rayleigh–Ritz model for the buckling and postbuckling of delaminated struts is presented, which performs well in terms of both accuracy and simplicity when compared with others from the literature (see Ref. 3 or 4, for example). Propagation of a system that already includes a delamination (see, for instance, Refs. 5–8) is not dealt with in the present paper, although it is understood that propagation must be significantly influenced by the postbuckling characteristics of interest here.[9,10]

The model reduces to three linked nonlinear cubic equations, produced with the help of the algebraic manipulation program Maple.[11] Full numerical solutions over a range of geometries, as described in greater detail in a companion paper,[12] are compared with output from the finite element analysis (FEA) code ABAQUS. Parametric variations include the relative length and depth of the delamination. The presence of secondary bifurcations, where the response switches from a closing to an opening mode, defines a critical delamination depth for any chosen length. Over the range of structural geometries where mixed-mode buckling becomes an issue, the underlying compound (double) bifurcation point indicates that a number of possible equilibrium states may lie close to each other. Under such circumstances the FEA solution technique is found to be highly sensitive to the choice of initial imperfection and could readily be coaxed into either of two alternative equilibrium states, for example. This raises a significant area of concern in the application of standard FEA codes to other problems with possible multiple solutions. Without other sources of information such as experimental data, how is the analyst expected to know whether his proposed solution is the one that the physical structure would actually be likely to trace?

II. Nonlinear Rayleigh–Ritz Formulation

The system shown in Fig. 1 comprises two undelaminated regions of length SL, separated by a region of delamination of length L. Differential stretching between laminates generates nonlinear effects not dissimilar to those of plates and shells. Separate laminates are therefore given both bending (EI) and in-plane (EA) stiffness, whereas the undelaminated parts are modeled with bending stiffness alone. The formulation over the delaminated part thus contrasts with a normal strut formulation, for which in-plane stretching can be ignored without losing anything of phenomenological significance.

Two significant modeling constraints apply at the ends of the delaminated region. First, rotations of the undelaminated part and each of the laminates must be the same at the join; second, there must be no relative shearing movement between laminates at the interface. The first constraint is enforced by the choice of a single degree of freedom (Q_3) to describe the end rotations, whereas the second ties the amount of axial stretching in each of the laminates to a second degree of freedom representing the total end shortening over the delaminated region, Δ. The buckling displacement of each laminate, represented by its clamped-end buckling mode, supplies two further degrees of freedom and provides a Rayleigh–Ritz model in the spirit of the frame analysis of Jennings.[13] With x_1 and x_2 measuring along the center line of each laminate as shown in Fig. 2, lateral displacements of the laminates can be described by

$$w_i = Q_i \sin^2(\pi x_i/L) + Q_3(1/L)x_i(L - x_i) \qquad (1)$$

($i = 1$ or 2) for the delaminated parts and

$$w_3 = Q_3 \frac{\sin \beta x_3}{\beta \cos \beta SL}, \qquad \text{where} \qquad \beta = \sqrt{\frac{12P}{Et^3}} \qquad (2)$$

for the undelaminated parts, x_3 being measured from the pinned supports. The latter is chosen to match both the deflection and the end rotation condition at $x_3 = SL$, in a portion of an equivalent undelaminated strut.

Presented as Paper 2003-1462 at the AIAA/ASME/ASCE/AHS/ASC 44th Structures, Structural Dynamics, and Materials Conference, Norfolk, VA, 7–10 April 2003; received 22 October 2003; revision received 20 April 2004; accepted for publication 30 April 2004.

*Professor of Structural Mechanics, Department of Mechanical Engineering.
†Research Officer, Department of Mechanical Engineering.
‡Senior Lecturer in Aerospace Structures, Department of Mechanical Engineering. Member AIAA.
§Professor of Material Science, Department of Engineering and Applied Science.
¶Research Student, Department of Mechanical Engineering.

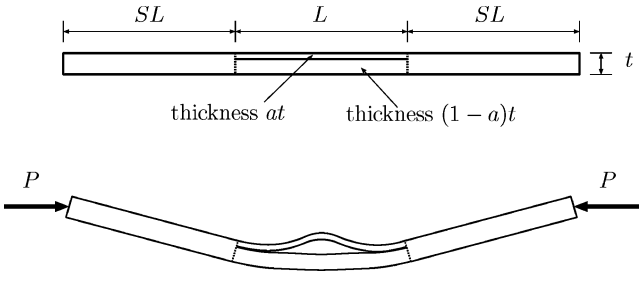

Fig. 1 Strut delamination model.

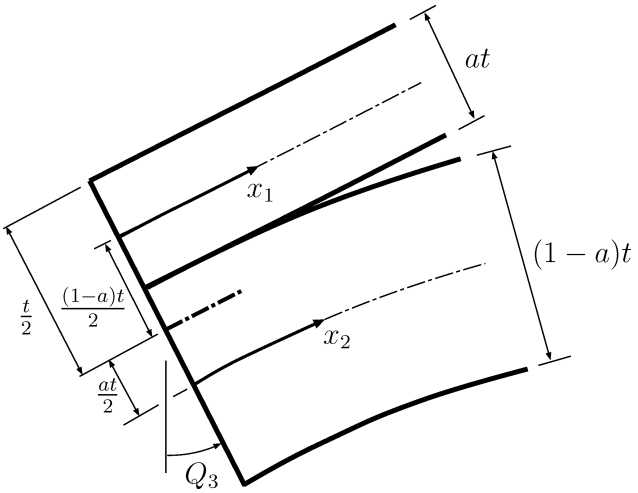

Fig. 2 Geometry at ends of delaminated region.

Under the assumption that each of the laminates is in a state of simple bending about its own neutral axis, the first-order strain energy of bending is

$$U_B = \frac{1}{24}Et^3\left[a^3\int_0^L\left(\frac{\mathrm{d}^2w_1}{\mathrm{d}x_1^2}\right)^2\mathrm{d}x_1 + (1-a)^3 \times\int_0^L\left(\frac{\mathrm{d}^2w_2}{\mathrm{d}x_2^2}\right)^2\mathrm{d}x_2 + 2\int_0^S\left(\frac{\mathrm{d}^2w_3}{\mathrm{d}x_3^2}\right)^2\mathrm{d}x_3\right]$$

The total axial shortening in each of the laminates can be written as

$$\delta_1 = \Delta - \frac{1}{2}\int_0^L\left(\frac{\mathrm{d}w_1}{\mathrm{d}x_1}\right)^2\mathrm{d}x_1 - (1-a)tQ_3$$

$$\delta_2 = \Delta - \frac{1}{2}\int_0^L\left(\frac{\mathrm{d}w_2}{\mathrm{d}x_2}\right)^2\mathrm{d}x_2 + atQ_3$$

With the assumption that the corresponding strains are evenly distributed along the length L, the total stretching energy of the system is

$$U_S = \tfrac{1}{2}(Et/L)\left[a\delta_1^2 + (1-a)\delta_2^2\right]$$

This is the source of all of the nonlinear terms.

A final contribution to the total potential energy comes from the work done by the load P moving through its corresponding deflection $\mathcal{E}$:

$$V = U_B + U_S - P\mathcal{E} \tag{3}$$

where

$$\mathcal{E} = \Delta + \int_0^{SL}\left(\frac{\mathrm{d}w_3}{\mathrm{d}x_3}\right)^2\mathrm{d}x_3 \tag{4}$$

the final term describing the end shortening of the two undelaminated regions. After substituting the deflected forms (1) into the preceding, a four-degree-of-freedom potential function $V(Q_1, Q_2, Q_3, \Delta, P)$ is obtained. Reduction of this function is carried out first by the elimination of Δ as a "passive" coordinate,[14] by solving the partial equilibrium equation $\partial V(Q_i, \Delta, P)/\partial\Delta = 0$ with respect to Δ and substituting the resulting expression into V (Ref. 12). This reduces V to the three-degree-of-freedom form $V(Q_i, P)$ $(i = 1, 2, 3)$. All calculations have successfully been carried out in the algebraic manipulation program Maple.[11]

III. Linear Eigenvalue Analysis

A. Eigenvalues and Eigenvectors

If total potential energy function is seen as a Taylor expansion about the fundamental equilibrium path F, where $Q_i = 0$ (Ref. 14), the quadratic coefficients can be written as

$$V_{11}^F = \tfrac{1}{6}Ea^3t^3L(\pi/L)^4 - \tfrac{1}{2}PaL(\pi/L)^2$$

$$V_{22}^F = \tfrac{1}{6}E(1-a)^3t^3L(\pi/L)^4 - \tfrac{1}{2}P(1-a)L(\pi/L)^2$$

$$V_{33}^F = \tfrac{1}{3}(Et^3/L) - \tfrac{1}{3}P\left[L + \sqrt{3Et^3/P}\,\tan\left(2\sqrt{3}\,SL\sqrt{P/Et^3}\right)\right]$$

$$V_{12}^F = 0, \qquad V_{13}^F = -Pa, \qquad V_{23}^F = -P(1-a) \tag{5}$$

where subscripts denote partial differentiation with respect to the corresponding degree of freedom. Critical loads P^C are obtained from setting the determinant $|V_{ij}^C| = 0$, and corresponding critical modeshapes can then be obtained directly from the associated eigenvectors[2]:

$$Q_1/Q_3|^C = -V_{13}/V_{11}|^C, \qquad Q_2/Q_3|^C = -V_{23}/V_{22}|^C \tag{6}$$

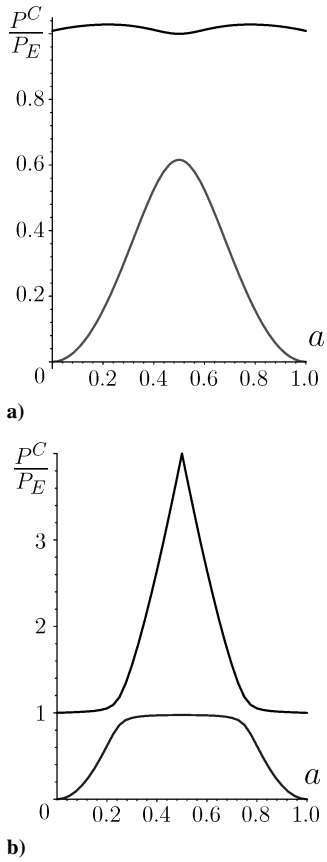

Fig. 3 Critical loads against delamination depth: S = a) 0 and b) 0.5.

Variations of the lowest two critical loads with delamination depth parameter a are shown in Fig. 3, normalized against the Euler load

$$P_E = \pi^2 EI/L^2(1+2S)^2 \tag{7}$$

of the corresponding undelaminated strut of length $L(1+2S)$. Figure 3a shows the lowest two critical loads for a full length delamination and Fig. 3b the equivalent for a centrally positioned half-length delamination. Mode shapes over the delaminated part in each case are shown in Fig. 4. The shape of Fig. 4b, with the midpoints of the two laminates moving in opposite directions as the buckling develops, will be referred to as the "opening" mode; by analogy, the shape of Fig. 4a will be called the "closing" mode shape, although this is strictly speaking a misnomer because although the layers move in the same direction, they do in fact separate. The closing mode always occurs at a lowest critical load, although the opening configuration is found to play a significant role in the postbuckling, as will be seen later.

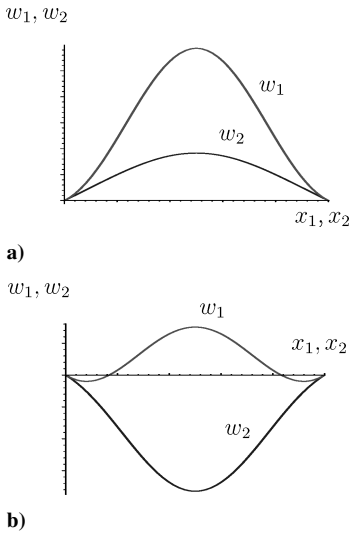

Fig. 4 Mode shapes for a full-length delamination ($S = 0$): a) first mode (closing) and b) second mode (opening).

In Fig. 3b, a change is seen to take place about $a = 0.25$. If a is less than this value the response is largely dominated by thin-film buckling in the thinner laminate; if a is greater and we move into the flat central region, the Euler load (7) is almost reached and the delamination is apparently less important. However, this may be at the cost of highly unstable postbuckling, as will be seen later.

B. Comparisons with FEA

For comparison purposes we also present the results based on critical load ABAQUS runs.[15] Here, the delaminated strut has been modeled using 88 Euler–Bernoulli beam elements (B23) with two nodes and three active degrees of freedom per node (two translations and a rotation). Interface elements, as used, for example, by Remmers and de Borst,[16] were not required, the possibility for propagation being omitted at this stage; however, the extension to propagating delamination is considered in a conpanion contribution.[9] The delaminated region was connected to the undelaminated regions by rigid arms, and the strut was given a thickness-to-length ratio $t/L(2S+1) = 0.1$. The critical buckling results are shown in Fig. 5. It can be seen that the lower curve, representing the pin-ended strut, compares well with the lower curve of Fig. 3b. The upper curve, however, gives the critical load of a strut with clamped ends. The comparisons underline that, where thin-film buckling is concerned, critical loads for pinned and clamped-end conditions are effectively the same. For higher values of a, the clamped results increase to a maximum at $a = 0.5$, which is well below the undelaminated value of $P^C = 4P_E$.

IV. Postbuckling Analysis

Optimization schemes are usually geared toward finding minima of objective functions, saddles and maxima being seen as of less interest. Here, however, we are interested in equilibrium states that are saddle points in V, unstable under dead loading conditions but likely to be stable when end shortening is controlled. To find such states numerically, we replace the search in V by a search in F, where

$$F = V_1^2 + V_2^2 + V_3^2 \tag{8}$$

subscripts denoting partial differentiation with respect to the corresponding degree of freedom as before. It can readily be demonstrated

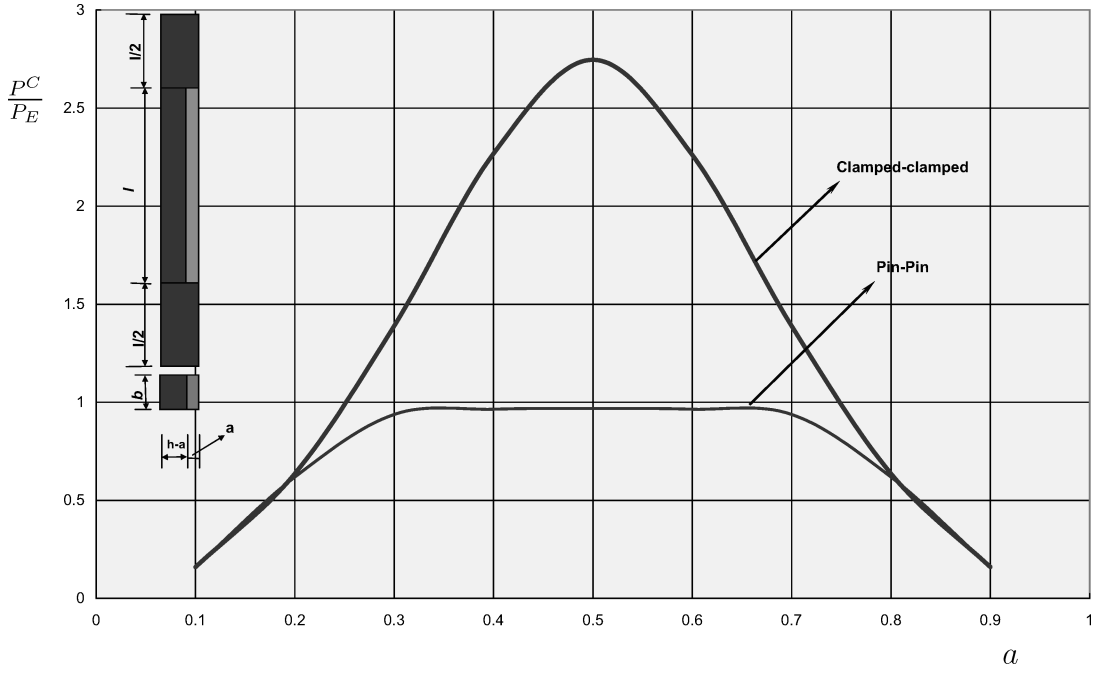

Fig. 5 Critical load ABAQUS results for pin-ended and clamped struts (cf. Fig. 3b).

that the equilibrium equations $V_i = 0$ $(i = 1, 2, 3)$ translate directly to $F_i = 0$. Moreover, if a diagonalized (modal) representation of V is employed,[14] F is also diagonalized, with the coefficients on the major diagonal appearing as the squares of the corresponding terms of V (Ref. 12). Thus saddles in V are replaced by minima of F, as shown schematically in the contour plots of Fig. 6, and standard optimization procedures are available for use on F. Having found the equilibrium paths for a particular configuration of S and a, the technique of homotopy then allows the paths readily to be traced for new values of these parameters, by tracking under their slow variation.[12]

A. Stable and Unstable Postbuckling

Two typical postbuckling forms are given in Fig. 7, on a plot of load P against its corresponding deflection $\mathcal{E}$ of Eq. (4), each normalized with respect to its corresponding Euler value. In each case the critical point, marked with an $\times$, has the general form of an asymmetric bifurcation.[14,17] Stiffness at the bifurcation point is the same for both the pre- and the postbuckling paths, although the latter tends to veer away from linearity as deflections grow. Both branches of the postbuckling solution are given, although the lower curves, shown as dashed lines, suggest that the laminates pass through one another and are thus unreachable.

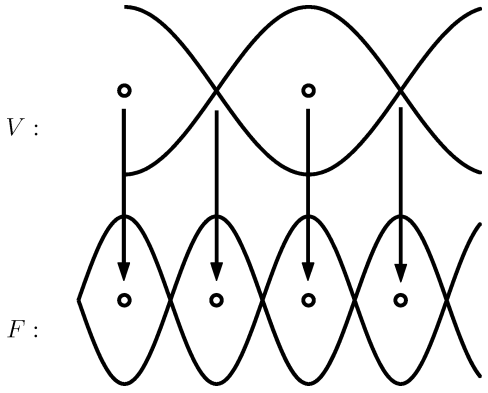

Fig. 6 Schematic representation of transformation from *V* to *F*.

The initial buckling mode, plotted in the inset diagrams with an $\times$, has in each case Q_1, Q_2, and Q_3 all positive. However, as the postbuckling develops, deflections in Q_2 and Q_3 may reverse (insets marked by a bullet). The drop in stiffness in the buckled laminate shifts the neutral axis of the combined section away from the side that has buckled, giving an effective offset in load that eventually will tend to push the laminates apart.[4] However, this effect may be counteracted by the natural moment produced by the combination of load P and rotation Q_3 acting in the opposite sense, as will be seen later.

B. Opening and Closing Responses

For small a, the initial postbuckling response is dominated by the buckling of the thinner laminate alone, described in the literature as thin-film buckling.[18,19] Figure 8a gives the response for full-length delamination and $a = 0.1$. The critical point, again marked by an $\times$, occurs early in the loading process but is followed by an extended region of stable postbuckling, in which initially the unbuckled laminate remains virtually straight. Here only the reachable stable branch of the postbuckling solution is shown. The initial buckling mode, shown over the delaminated region, again has Q_1, Q_2, and Q_3 all positive but with a much exaggerated Q_1 component. As before, because of an effective shift in the neutral axis, deflections in Q_3 finally reverse as the buckling develops, suggesting a tendency for the laminates to open.

This can be contrasted with the case of Fig. 8b. Now the postbuckling passes over a limit point, from where it would snap dynamically under dead load, but subsequently reaches a state where the laminates contact together, as shown by the bullet. The combination of P and positive Q_3 has overcome the shift in the neutral axis. Under a rigid loading condition this implies a stable response very like that of Euler buckling, and we refer to it as *overall buckling*.

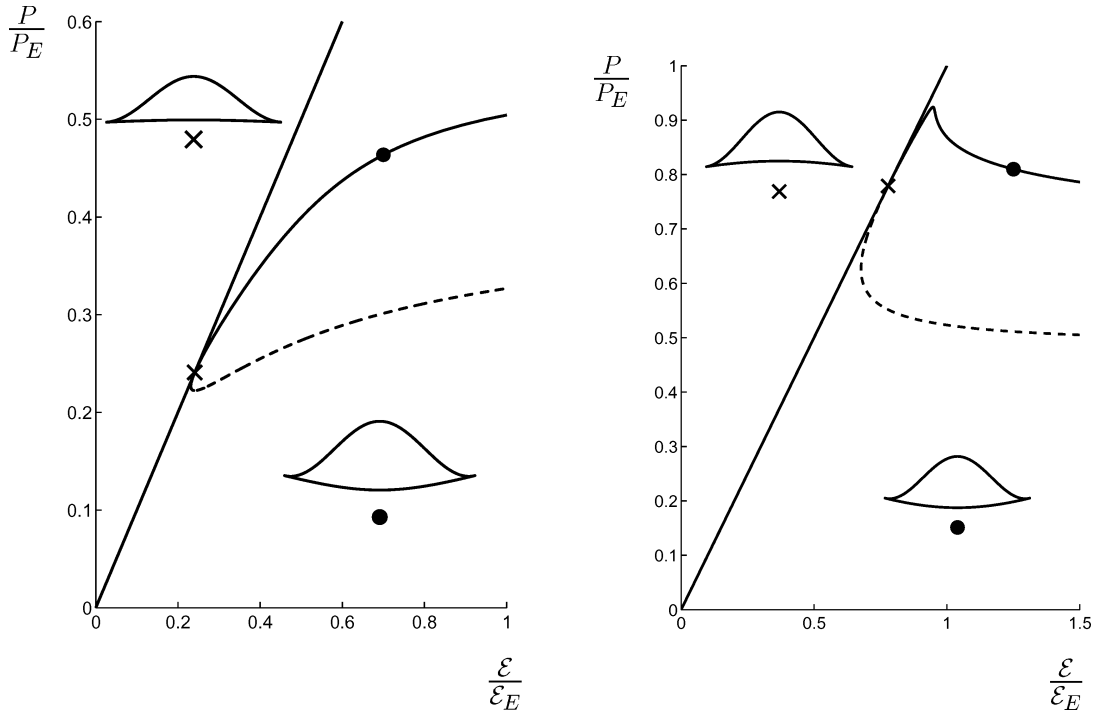

Fig. 7 Fundamental path and typical postbuckling responses: a) stable response for a full-length delamination ($S = 0$) at $a = 0.25$ and b) unstable response following a limit point for a half-length delamination ($S = 0.5$) at $a = 0.23$ (mixed-mode buckling).

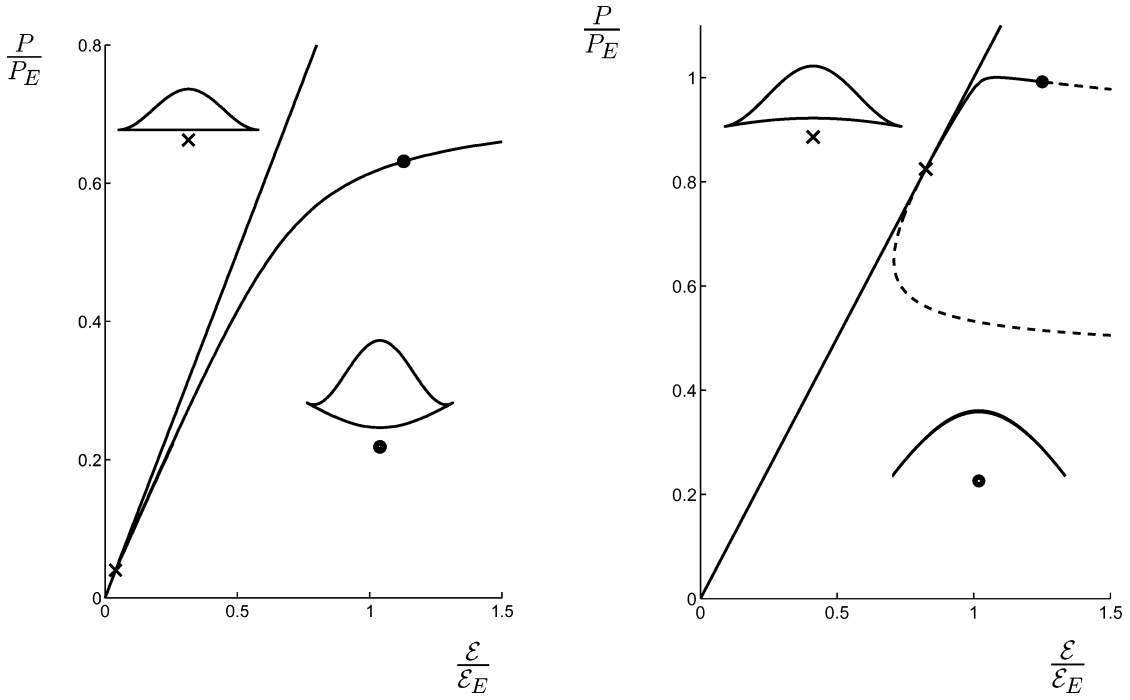

Fig. 8 Typical postbuckling responses: a) thin-film buckling at $S = 0$ and $a = 0.1$ and b) overall buckling at $S = 0.5$ and $a = 0.24$.

The two extremes of Figs. 8a and 8b are joined by a third possibility, shown in Fig. 7b. Here the response reaches a more severe limit point than for overall buckling and subsequently opens. We regard this response as potentially the most dangerous of the three possibilities from both buckling and fatigue viewpoints and refer to it as *mixed-mode buckling*. It tends to occur at values of a where the two lowest critical loads are closest together, as seen in Fig. 3.

C. Secondary Bifurcation and Critical Delamination Depth

The two plots of Figs. 7b and 8b come from similar geometries ($S = 0.5$; $a = 0.23$ and 0.24, respectively) yet show quite different responses: one opens, whereas the other closes. The changeover takes place at a secondary bifurcation point somewhere in the range $0.235 < a < 0.236$, as shown by Fig. 9. Here two sets of equilibrium paths are given at each value of a. As before, a broken line denotes an unreachable state where the laminates pass through one another, and a dot–dash line is used to distinguish the path that is disconnected from the critical point of interest. The switch from one form of behavior to the other is clearly seen. We shall refer to the value of a where the secondary bifurcation occurs as the *critical delamination depth*.

The equivalent set of curves for $S = 0$ given in Fig. 10 shows very similar behavior, but with one important difference. Whereas the closing configuration for $S = 0.5$ occurs on a rising stable postbuckling path, now it occurs after a limit point has been reached and the load has started to fall. This is an awkward response with regard to stability. Under controlled (dead) loading conditions, stability would be lost at the limit point and the system would snap dynamically to some far-field (undefined) equilibrium state. Under controlled end shortening (rigid loading) on the other hand, it would move in controlled fashion to the point marked by the bullet where the laminates come into contact, and a new (undefined but clearly stable) equilibrium path would be followed.

V. Comparison with Finite Element Solutions

It is well known that finite element codes can run into difficulties close to bifurcation points. When a primary bifurcation is expected, the introduction of small initial imperfections in the corresponding mode shape is often used to overcome such problems. However, a secondary bifurcation is likely to be more difficult to predict and consequently more of a problem to deal with. The corresponding mode shape may be intuitively less obvious, and there is a danger of the code either tracking the wrong equilibrium path or stopping completely. Both problems were encountered during the following comparative runs.

Figures 11a and 11b show comparisons of the present four-degree-of-freedom model with ABAQUS Standard[15] formulations for the two situations of Figs. 9 and 10. It should be noted that, to avoid introducing an extra unnecessary degree of freedom associated with end shortening in the undelaminated regions, the in-line stiffness in such regions was originally modeled as infinite. To enable comparisons with the finite element solutions, the extra end shortening associated with a material of Young's modulus E has been computed and added to the plots, but otherwise these mirror the responses given earlier. The ABAQUS runs were performed using a total of 160 Euler–Bernoulli two-node cubic (B23) beam elements, with three active degrees of freedom per node as before. The Riks arc length method was employed for all postbuckling solutions.

The comparisons demonstrate clearly that the four-degree-of-freedom model captures the postbuckling responses correctly, both qualitatively and quantitatively. They also indicate complete agreement in the location of the secondary bifurcation at the critical delamination depth. It was found that the asymmetry of the delamination within the thickness acted to round off the initial bifurcation, and so no extra imperfection was ever required in the initial mode shape. However, the situation close to the secondary bifurcation proved to be more of a problem, as expected. In three of the finite element runs, no imperfection was required to obtain satisfactory results, but for $S = 0.5$ and $a = 0.38$, without an imperfection in the second mode shape, the finite element solution stopped completely at the secondary bifurcation point. A small imperfection of $0.005t$ in the buckled shape w_1 of the upper laminate was found to be sufficient to overcome this problem. By introducing other small imperfection shapes, it was also found that the finite element routines were relatively easy to coax

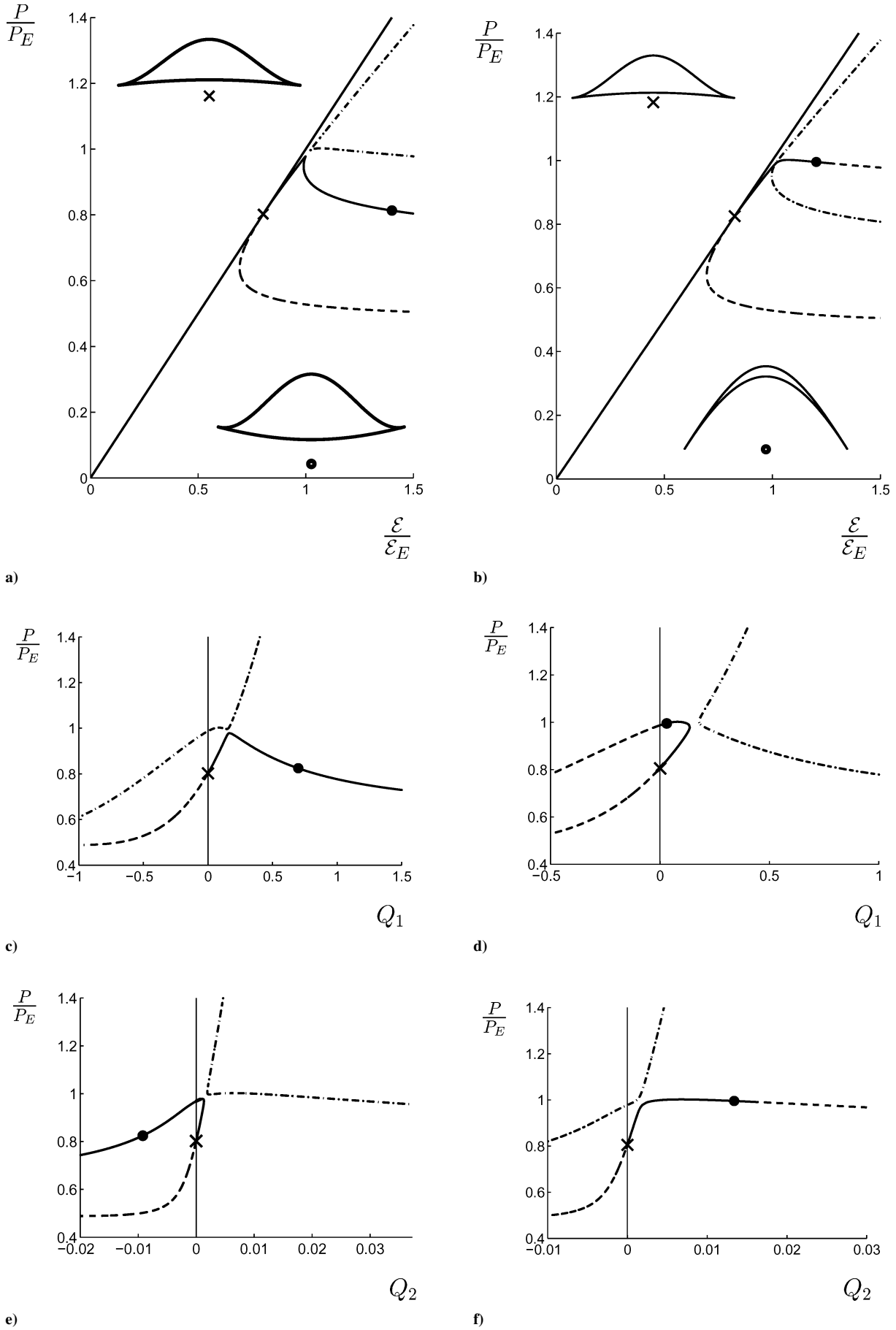

Fig. 9 Typical load/deflection plots either side of the secondary bifurcation point for $S = 0.5$ ($L = 55$ and $t = 2.13$): a), c); and e), $a = 0.235$; and b), d), and f), $a = 0.236$.

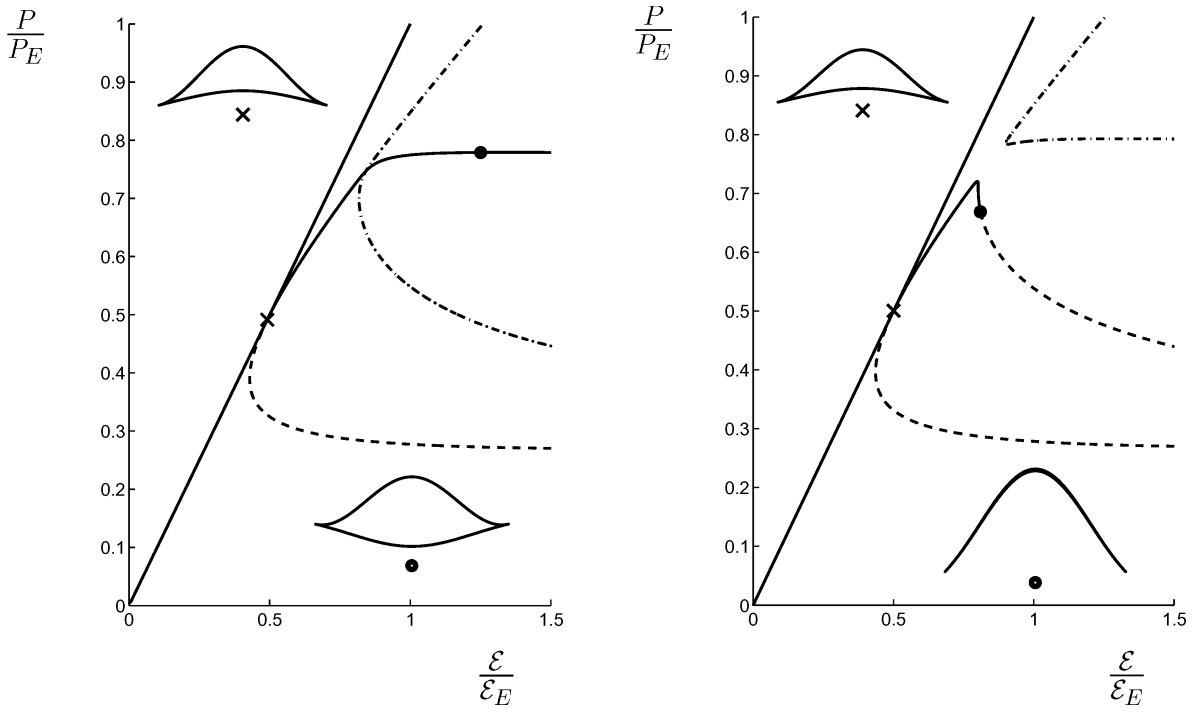

a) b)

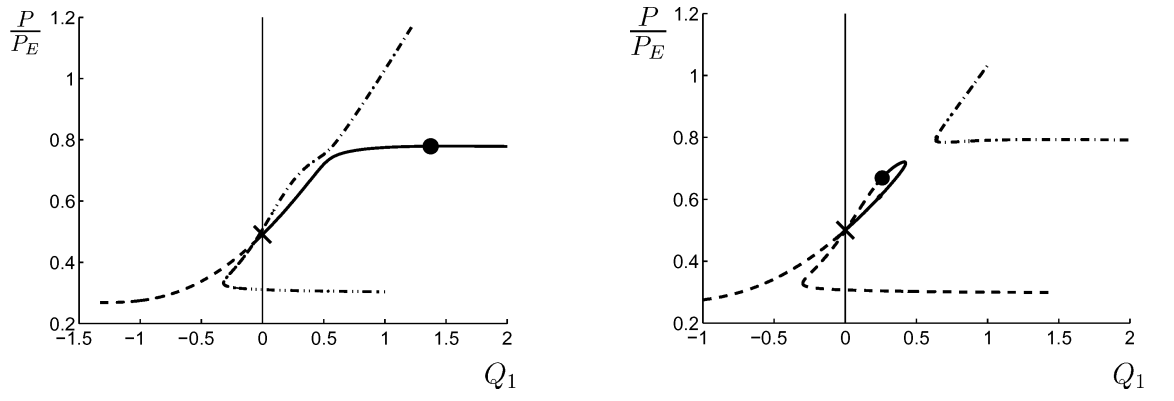

c) d)

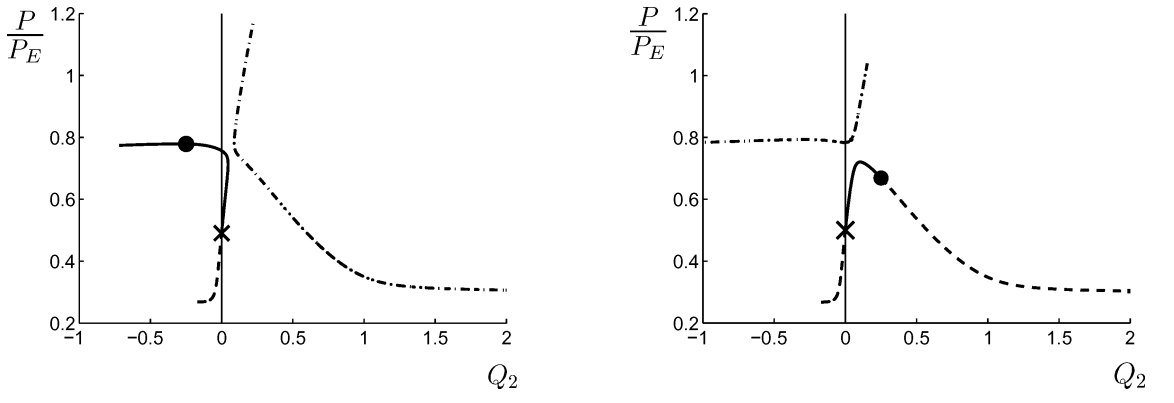

e) f)

Fig. 10 Typical load/deflection plots either side of the secondary bifurcation point for $S = 0$ ($L = 55$ and $t = 2.13$): a), c), and e), $a = 0.38$; and b), d), and f), $a = 0.385$.

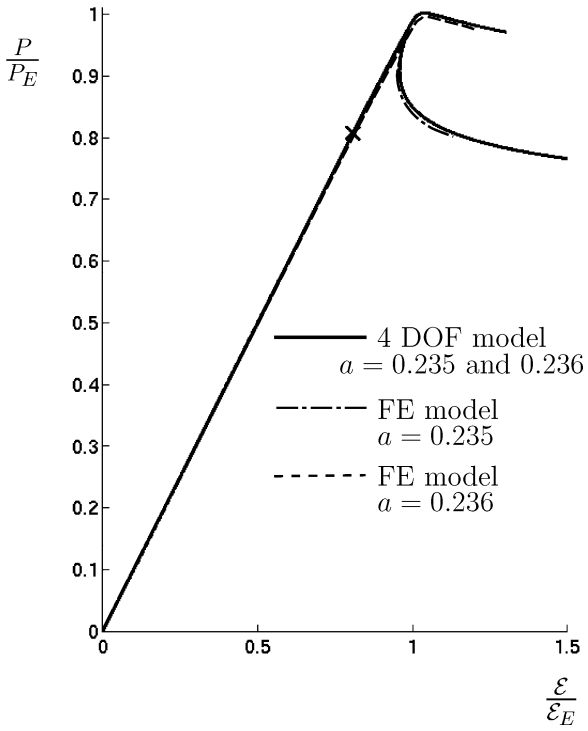

a)

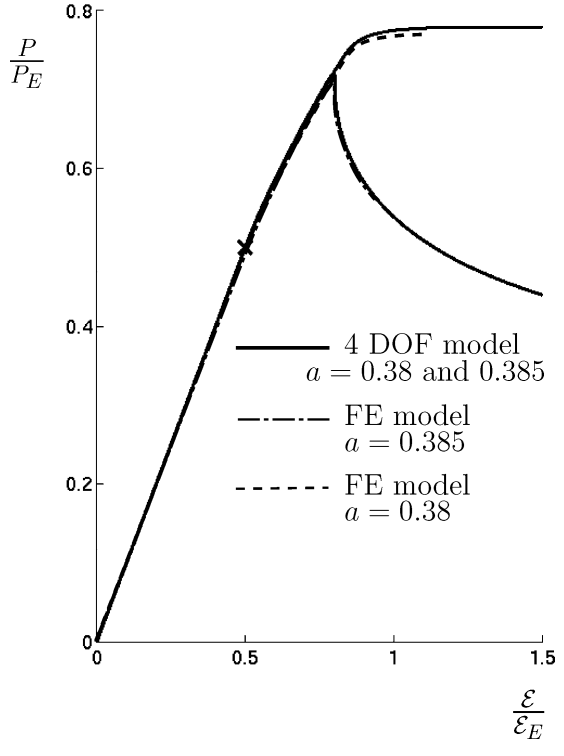

b)

Fig. 11 Comparison of the present analysis with output from ABAQUS Standard: a) $S = 0.5$, $a = 0.235$ and 0.236; and b) $S = 0$, $a = 0.38$ and 0.385.

down the wrong postbuckling route. Such behavior underlines the point that standard finite element packages can easily be misled into choosing an equilibrium path that would be unlikely to be traced in practice.

VI. Conclusions

The nonlinear four-degree-of-freedom delaminated strut model developed here shows that, depending on the position and length of the delamination, a wide variety of postbuckling behaviors can result. Thin-film buckling is seen to be platelike and stable over the initial postbuckling range, for example, but mixed-mode buckling near the critical delamination depth is unstable and shell-like. In all cases, initial buckling has the laminates moving in the same direction, but as the postbuckling develops the thicker laminate can reverse direction and the laminates tend to move apart; in a fatigue environment, this might be seen as a relatively dangerous circumstance. The comparisons with the finite element ABAQUS runs demonstrate that the model is able to capture fully the postbuckling behavior over large deflections.

The difficulties experienced by finite element routines such as ABAQUS Standard are highlighted at the end of the paper. Such problems are of course fully overcome by taking stability as well as equilibrium into account. We would therefore not expect them with dynamical time-stepping routines, as used in ABAQUS Explicit, for example. However, although reliable in this sense, such numerical procedures can be expensive in terms of both effort and computer time.

The kind of analysis presented here is designed to play a different but entirely complementary role. It focuses on the phenomenology, asking the question, for example, In how many different ways can the system lose its stability, and how are these linked to the multiplicity of solutions that results? The objective is to answer in a manner that highlights the full range of possible outcomes. We note that Rayleigh–Ritz approaches such as this have been used with success for other formulations of delamination (and seen, for example, as ". . . simple, inexpensive, and accurate, except for highly anisotropic regions"[10]), although usually only in a linear context. If the mode shapes are chosen with care, such methods can be extended relatively painlessly, and certainly accurately, into the nonlinear regime. Moreover, being based on the concept of total potential energy, questions of stability are automatically answered via the classical "rolling ball analogy" (see, for example, Ref. 14).

Acknowledgments

This work has been conducted with support from the U.K. Engineering and Physical Sciences Research Council (Grant GR/R54828) and Westland Helicopters, Ltd.

References

[1]Koiter, W. T., and Pignataro, M., "A General Theory for the Interaction Between Local and Overall Buckling of Stiffened Panels," Dept. of Mechanical Engineering, Delft Univ. of Technology, TR WTHD 83, Delft, The Netherlands, 1976.

[2]Thompson, J. M. T., and Hunt, G. W., *Elastic Instability Phenomena*, Wiley, Chichester, England, U.K., 1984, pp. 164–194.

[3]Kachanov, L. M., *Delamination Buckling of Composite Materials*, Kluwer Academic Publishers, Dordrecht, The Netherlands, 1988.

[4]Yin, W. L., Sallam, S. N., and Simitses, G. J., "Ultimate Axial Load Capacity of a Delaminated Beam-Plate," *AIAA Journal*, Vol. 24, No. 1, 1986, pp. 123–128.

[5]Whitcomb, J. D., "Parametric Analytical Study of Instability-Related Delamination Growth," *Composite Science and Technology*, Vol. 25, No. 1, 1986, pp. 19–48.

[6]Kardomateas, G. A., "The Initial Post-Buckling and Growth Behavior of Internal Delaminations in Composite Plates," *Journal of Applied Mechanics*, Vol. 60, No. 4, 1993, pp. 903–910.

[7]Chattopadhyay, A., and Gu, H., "New Higher Order Plate Theory in Modeling Delamination Buckling of Composite Laminates," *AIAA Journal*, Vol. 38, No. 8, 1994, pp. 1709–1716.

[8]Kardomateas, G. A., and Huang, H., "The Initial Post-Buckling Behavior of Face-Sheet Delaminations in Sandwich Composites," *Journal of Applied Mechanics*, Vol. 70, No. 2, 2003, pp. 191–199.

[9]Hu, B., Butler, R., Almond, D. P., and Hunt, G. W., "Post-Buckling and Fatigue Limit of Artifically Delaminated Composites," *Proceedings of the 45th AIAA/ASME/ASCE/AHS/ASC Structures, Structural Dynamics, and Materials Conference* [CD-ROM], AIAA, Reston, VA, 2004.

[10]Shivakumar, K. N., and Whitcomb, J. D., "Buckling of a Sublaminate in a Quasi-Isotropic Composite Laminate," *Journal of Composite Materials*, Vol. 19, No. 1, 1985, pp. 2–18.

[11]Monagan, M. B., Geddes, K. O., Heal, K. M., Labahn, G., and Vorkoetter, S. M., *Maple V Programming Guide*, Springer, London, 1998.

[12]Wright, J. E., "Compound Bifurcations in the Buckling of a Delaminated Composite Strut," *Nonlinear Dynamics* (to be published).

[13]Jennings, A., "The Elastic Stability of Rigid-Jointed Frames," *International Journal of Mechanical Sciences*, Vol. 5, No. 1, 1963, pp. 99–113.
[14]Thompson, J. M. T., and Hunt, G. W., *A General Theory of Elastic Stability*, Wiley, London, 1973.
[15]*ABAQUS/Standard User's Manual*, Ver. 6.3, Hibbitt, Karlsson and Sorensen, Inc., Pawtucket, RI, 2002.
[16]Remmers, J. J. C., and de Borst, R., "Delamination Buckling of Fibre-Metal Laminates," *Composite Science and Technology*, Vol. 61, No. 15, 2001, pp. 2207–2213.
[17]Golubitsky, M., Stewart, I., and Schaeffer, D. G., *Singularities and Groups in Bifurcation Theory, Volume II*, Vol. 51, Applied Mathematical Sciences, Springer-Verlag, New York, 1988.
[18]Chai, H., Babcock, C. D., and Knauss, W. G., "One Dimensional Modelling of Failure in Laminated Plates by Delamination Buckling," *International Journal of Solids and Structures*, Vol. 17, No. 11, 1981, pp. 1069–1083.
[19]Simitses, G. J., Sallam, S., and Yin, W. L., "Effect of Delamination of Axially Loaded Homogeneous Laminated Plates," *AIAA Journal*, Vol. 23, No. 9, 1985, pp. 1437–1444.

K. Shivakumar
Associate Editor